Available online at www.sciencedirect.com
SCIENCE DIRECT®
PERGAMON
International Journal of Heat and Mass Transfer 46 (2003) 2875–2886
International Journal of HEAT and MASS TRANSFER
www.elsevier.com/locate/ijhmt

Simultaneous heat and mass transport in paper sheets during moisture sorption from humid air

W.R. Foss [1], C.A. Bronkhorst [*,2], K.A. Bennett

Weyerhaeuser Company, Federal Way, WA 98063-9777, USA

Received 21 June 2002; received in revised form 17 December 2002

Abstract

A model of simultaneous heat and mass transfer through a porous material is presented to explain transient moisture sorption by paper sheets from humid air. There are three primary resistances to moisture transport: (1) diffusion through an external boundary layer; (2) diffusion through the pore system and, (3) diffusion from the pore system into the fibers. It is found that diffusion through the fiber phase perpendicular to the plane of the sheet is not significant for the moisture content range considered here. The mass transport model is able to predict the results of transverse moisture gradient experiments which show that moisture content gradients in paper are not as large as previously thought during transient periods. The model shows that the sigmoidal temperature response of paper to a linear change of relative humidity is due to non-linearities of the moisture content isotherm and heat of sorption.

1. Introduction

Paper is a porous composite material constructed from chemically and mechanically processed wood fibers which are self binding when dried from a wet state. In their uncollapsed condition, these fibers are cylindrical in geometry with an open lumen in the interior and, although highly variable, have a length on the order of 2 mm, a diameter on the order of 30 μm and a wall thickness on the order of 5 μm. Each fiber is itself a cellulosic fiber composite with predominantly crystalline cellulose fibrils embedded in a matrix of amorphous lignin and hemicellulose. Although once again highly variable, each fiber has a crystallinity on the order of two-thirds. Only the amorphous hemicellulose polymer is hygrophilic. Even when plasticized by water, the packing efficiency of these fibers is generally quite low with minimum practical porosity on the order of 0.5.

Transient sorption of moisture from humid air is of interest because of the effect of moisture on the mechanical properties of paper [1] and its dimensional stability [2,3]. Recently, intense interest has been focused on this subject because of the dramatic degradation of paper strength caused by the mechano-sorptive effect and other moisture transient phenomena [4,5]. These effects result from the repeated uptake and release of moisture by sheets in response to cyclic humidity environments and is responsible for significantly shorter lifetimes of paper packaging products in uncontrolled environments. Conventional theories of moisture diffusion prove ineffective at explaining the duration and shape of sorption transients [6], and therefore cannot be trusted to help describe accelerated creep, mechano-sorption, hygroexpansion, or the later stages of the web drying process in paper production.

2. Theory

Models of transient moisture sorption by paper must account for the porous nature of the material. Lescanne

* Corresponding author.
E-mail addresses: wfoss@ca.nektar.com (W.R. Foss), cabronk@lanl.gov (C.A. Bronkhorst).
[1] Now with Nektar Therapeutics, 150 Industrial Rd, San Carlos, CA 94070, USA. Tel.: +650-631-3309; fax: +650-631-3150.
[2] Now with Los Alamos National Laboratory, Theoretical Division, Mail Stop B216, Los Alamos, NM 87545, USA. Tel.: +505-665-0122; fax: +505-665-5926.

0017-9310/03/$ - see front matter
doi:10.1016/S0017-9310(03)00052-8

Nomenclature

a, b	half-thickness of the average pore space and fiber wall, m
a_s	pore interfacial area per unit volume of sheet, 1/m
a_w	activity of water in the gas phase
A	parameter in the high humidity term of moisture content isotherm
β_f, β_p	interphase transport parameters
C	BET isotherm parameter
$\widehat{C}_{p,f}$, $\widehat{C}_{p,p}$	fiber and pore phase specific heats, J/kg/K
D_f, D_p	diffusivity of water in the fiber and pore phases, m^2/s
D_p^*	dimensionless pore phase diffusivity
ε	paper porosity
ΔH_{abs}	differential heat of absorption, J/kg
ΔH_{prim}	heat of absorption of water onto primary sites, J/kg
ΔH_{cond}	heat of condensation, J/kg
K_{eq}	non-dimensional slope of moisture content isotherm
k_f, k_p	thermal conductivity of the fiber and pore phases, J/m/s/K
k_{eff}	effective thermal conductivity, J/m/s/K
k_{eff}^*	non-dimensional effective thermal conductivity
$K_{h,i}$	pore-to-fiber heat transfer coefficient, $J/m^2/s/K$
$K_{m,i}$	pore-to-fiber mass transfer coefficient, m/s
$K_{h,s}$	surface heat transfer coefficient, $J/m^2/s/K$
$K_{m,s}$	surface mass transfer coefficient, m/s
l	half-thickness of the sheet, m
M_w, M_a	molecular weight of water and air, kg/kmol
$N_{Bi,m}$, $N_{Bi,h}$	mass and heat transfer Biot numbers
N_{Le}	Lewis number
p_w	partial pressure of water, Pa
p^{sat}	saturation partial pressure of water, Pa
P	total pressure, Pa
ρ_f, ρ_p	density of the fiber and pore phases, kg/m^3
ρ_s	density of the sheet, kg/m^3
t	time, s
ψ	non-dimensional time
T	temperature, K
T_∞	temperature far from the sheet, K
T_f, T_p	temperature of fiber and pore phases, K
θ	non-dimensional temperature
θ_∞	non-dimensional temperature far from the sheet
τ_f, τ_p	fiber and pore phase tortuosities
ω_f, ω_p	mass fraction of moisture in the fiber and pore phases
$\bar{\omega}_f$, $\bar{\omega}_p$	mass fraction of moisture averaged over the width of the pore or fiber in the x-direction
$\omega_{f,0}$, $\omega_{p,0}$	initial mass fraction of moisture in the fiber and pore phases
$\omega_{f,\infty}$, $\omega_{p,\infty}$	final mass fraction of moisture in the fiber and pore phases
ω_f^*, ω_p^*	mass fraction of moisture in fiber and pore normalized by the initial and final values
ω_∞	mass fraction of moisture far from the sheet
ω_{eq}	equilibrium moisture content isotherm on a mass fraction basis
ω_{eq}^*	equilibrium moisture content isotherm normalized by initial and final values
ω_{mc}	mass fraction of absorbed water on a dry fiber basis
ω_{prim}	mass fraction of water bound to primary absorption sites on a dry fiber basis
ω_{mono}	mass fraction of water in the completely adsorbed monolayer on a dry fiber basis
x, x'	distance from the center of the pores and fibers parallel to the plane of the sheet, m
z	distance from the center of the sheet perpendicular to the plane of the sheet, m
ζ	non-dimensional distance in the z-direction

et al. [7] and Nilsson et al. [8] have demonstrated that z-direction moisture transport through sheets is dominated by water vapor diffusing through the open network of pores. Hence, moisture transport through the pore spaces is much more rapid than through the fibers. When considering the transient uptake of water by the fibers of a sheet, the humidity inside the pores and the moisture content of the fibers must be accounted for separately because they will not necessarily be in equilibrium.

Salin [9] and Cunningham [10] proposed two phase models of transient moisture transport in paper but their models do not include a detailed analysis of the pore-to-fiber mass transport. These authors also neglect the temperature change in sheets due to the heat of sorption, which alters the sorption kinetics through the temperature-dependent moisture content isotherms. More recently, Fan and Wen [11] and Fan et al. [12] have applied similar but more detailed two-phase models to heat and moisture transport in fibrous insulation and clothing. These models include interphase moisture transport as well as condensation and freezing of moisture on the fibers and radiative heat transfer. In this section, the equations of transient mass transport in the z-direction of paper sheets are outlined, the mass transfer in the pore-to-fiber direction is characterized

and the thermal energy balance is derived to account for the temperature change of the sheet and the mass–energy coupling of the moisture isotherms.

The mass balance of water vapor inside the pores, written in terms of the weight fraction of water, is

$$\frac{\partial \omega_p}{\partial t} = \frac{1}{\tau_p}\frac{\partial}{\partial z}\left(D_p \frac{\partial \omega_p}{\partial z}\right) - \frac{a_s K_{m,i}}{\varepsilon}[\omega_{eq}(\omega_p) - \omega_f] \tag{1}$$

The diffusion term represents the vapor diffusion in the direction of the tortuous path of the pore spaces. The last term represents the mass transport of vapor from the pores into the neighboring fibers. The interphase mass transfer coefficient, $K_{m,i}$, will be derived in terms of fundamental sheet properties below. The equilibrium moisture content of the fibers, ω_{eq}, will also be described below.

Similarly, the mass balance for moisture within the fibers is

$$\frac{\partial \omega_f}{\partial t} = \frac{1}{\tau_f}\frac{\partial}{\partial z}\left(D_f \frac{\partial \omega_f}{\partial z}\right) + \frac{a_s K_{m,i}\rho_p}{(1-\varepsilon)\rho_f}[\omega_{eq}(\omega_p) - \omega_f] \tag{2}$$

The porosity is found from the sheet and the fiber densities as $\varepsilon = 1 - \rho_s/\rho_f$. Many relationships have been proposed between the tortuosity of a pore system and the porosity. Akanni et al. [13] show that the most reliable of such relationships is

$$\tau = 1 - \frac{\ln \varepsilon}{2} \tag{3}$$

which may be applied to both the pores and the fibers, where, in the latter case, ε is replaced by $(1-\varepsilon)$. Later, experimental results will verify that the quantity

$$\frac{\tau_p(1-\varepsilon)\rho_f D_f}{\tau_f \varepsilon \rho_p D_p} \ll 1 \tag{4}$$

and so the z-direction diffusion in the fibers can be considered negligible. Hence, the diffusion term in Eq. (2) can be dropped and only two boundary conditions are required. For a sheet exposed to the same humidity transient on either side, there is a symmetry plane at the center

$$\left.\frac{\partial \omega_p}{\partial z}\right|_{z=0} = 0 \tag{5}$$

At the surface of the sheet, the resistance through the boundary layer above the sheet is accounted for with an external mass transfer coefficient

$$-\frac{\varepsilon D_p}{\tau_p}\left.\frac{\partial \omega_p}{\partial z}\right|_{z=l} = K_{m,s}[\omega_p|_{z=l} - \omega_\infty(t)] \tag{6}$$

where the humidity far from the sheet varies with time. The initial conditions are usually taken to be a sheet in equilibrium with the surrounding air

$$\omega_p(z,0) = \omega_\infty(0) \tag{7}$$

Initially, the fibers are considered to be in equilibrium with the humidity in the pores

$$\omega_f(z,0) = \omega_{eq}(\omega_p(z,0)) \tag{8}$$

The interphase mass transfer coefficient, $K_{m,i}$, is expressed in terms of measurable parameters by modeling the mass transport in the direction perpendicular to the pore–fiber interface, denoted here as the x-direction. Based on micrographs of cross-sections of paper sheets, the pores are best described by a slab-like geometry. For simplicity, the pores and fibers are assumed to be interleaved and to have uniform half-thicknesses of a and b, respectively, in the x-direction. With these assumptions, it can be shown that a_s, the interfacial area between pores and fibers, is equivalent to ε/a. At any position z in the pores, the x-direction moisture transport is expressed as

$$\left.\frac{\partial \omega_p(x)}{\partial t}\right|_z = \left.\frac{\partial}{\partial x}\left(D_p \frac{\partial \omega_p(x)}{\partial x}\right)\right|_z + \frac{1}{\tau_p}\frac{\partial}{\partial z}\left(D_p \frac{\partial \omega_p}{\partial z}\right) \tag{9}$$

where $x = 0$ at the centerline of the pore. The second term accounts for x-direction diffusion through the pore space and replaces the analogous pore-to-fiber transport term in Eq. (1). In the fibers, since the z-direction diffusion is considered negligible by the condition given in Eq. (4), the x-direction moisture transport is expressed as

$$\left.\frac{\partial \omega_f(x')}{\partial t}\right|_z = \left.\frac{\partial}{\partial x'}\left(D_f \frac{\partial \omega_f(x')}{\partial x'}\right)\right|_z \tag{10}$$

where x' is parallel with x and $x' = 0$ at the centerline of the fiber. At the pore–fiber interface, the moisture flux boundary condition is

$$\begin{aligned}\rho_p D_p \left.\frac{\partial \omega_p}{\partial x}\right|_{x=a} &= \rho_f D_f \left.\frac{\partial \omega_f}{\partial x'}\right|_{x'=b} \\ &= -\rho_p K_{m,i}[\omega_{eq}(\bar{\omega}_p) - \bar{\omega}_f]\end{aligned} \tag{11}$$

For consistency with Eqs. (1) and (2), the average pore and fiber moisture contents at any position z are used in the driving force term of Eq. (11). Also at the interface, local moisture equilibrium is assumed

$$\omega_f|_{x'=b} = \omega_{eq}(\omega_p|_{x=a}) \tag{12}$$

Since z-direction diffusion in the pores is rapid compared to the rate of moisture change in the fibers, the x-direction profiles remain relatively stable for short periods and a pseudo-steady state approximation is used to solve Eqs. (9) and (10). This yields parabolic moisture profiles in the x-direction

$$\omega_p(x) = \bar{\omega}_p - \frac{aK_{m,i}[\omega_{eq}(\bar{\omega}_p) - \bar{\omega}_f]}{2D_p}\left[\left(\frac{x}{a}\right)^2 - \frac{1}{3}\right] \tag{13}$$

and

$$\omega_{\mathrm{f}}(x') = \bar{\omega}_{\mathrm{f}} + \frac{b\rho_{\mathrm{p}}K_{\mathrm{m,i}}[\omega_{\mathrm{eq}}(\bar{\omega}_{\mathrm{p}}) - \bar{\omega}_{\mathrm{f}}]}{2\rho_{\mathrm{f}}D_{\mathrm{f}}}\left[\left(\frac{x'}{b}\right)^2 - \frac{1}{3}\right] \tag{14}$$

The driving force for mass transport between pore and fiber, $\omega_{\mathrm{eq}}(\bar{\omega}_{\mathrm{p}}) - \bar{\omega}_{\mathrm{f}}$, in Eqs. (13) and (14) is rewritten as:

$$\omega_{\mathrm{eq}}(\bar{\omega}_{\mathrm{p}}) - \omega_{\mathrm{f}} = [\omega_{\mathrm{eq}}(\bar{\omega}_{\mathrm{p}}) - \omega_{\mathrm{f}}|_{x'=b}] + [\omega_{\mathrm{f}}|_{x'=b} - \bar{\omega}_{\mathrm{f}}] \tag{15}$$

The driving force on the fiber side is approximated with a linearization of the moisture content isotherm about the interface condition and Eq. (15) becomes

$$\omega_{\mathrm{eq}}(\bar{\omega}_{\mathrm{p}}) - \bar{\omega}_{\mathrm{f}} \cong \left.\frac{\partial\omega_{\mathrm{eq}}}{\partial\omega_{\mathrm{p}}}\right|_{x=a}(\bar{\omega}_{\mathrm{p}} - \omega_{\mathrm{p}}|_{x=a}) + (\omega_{\mathrm{f}}|_{x'=b} - \bar{\omega}_{\mathrm{f}}) \tag{16}$$

The terms in parentheses in Eq. (16) are replaced with Eqs. (13) and (14), evaluated at the interface conditions. Now, the $\omega_{\mathrm{eq}}(\bar{\omega}_{\mathrm{p}}) - \bar{\omega}_{\mathrm{f}}$ term may be eliminated from Eq. (16) and from this the overall interphase mass transport coefficient may be found in terms of measurable material properties

$$K_{\mathrm{m,i}} = \frac{3\rho_{\mathrm{f}}D_{\mathrm{p}}D_{\mathrm{f}}}{b\rho_{\mathrm{p}}D_{\mathrm{p}} + a\rho_{\mathrm{f}}D_{\mathrm{f}}(\partial\omega_{\mathrm{eq}}/\partial\omega_{\mathrm{p}})|_{x=a}} \tag{17}$$

which has the form expected of two mass transfer resistances in series.

Based on the assumption of a slab-like geometry, the half-thickness of the pores can be found in terms of b and ε. The porosity can be expressed in terms of the thicknesses and the tortuosities as

$$\varepsilon = \frac{a\tau_{\mathrm{p}}}{a\tau_{\mathrm{p}} + b\tau_{\mathrm{f}}} \tag{18}$$

From here, it can be shown that

$$\frac{b}{a} = \frac{(1-\varepsilon)\tau_{\mathrm{p}}}{\varepsilon\tau_{\mathrm{f}}} = \frac{(1-\varepsilon)(2-\ln\varepsilon)}{\varepsilon[2-\ln(1-\varepsilon)]} \tag{19}$$

by application of Eq. (3). Now a can be estimated from b, where b is measured from electron micrographs of fiber cross-sections.

The equilibrium moisture content of the fibers is a function of both the relative humidity and temperature and is also dependent on their moisture content history. The primary absorption isotherms, namely the moisture contents approached in a monotonically increasing manner from a completely dry state, have a sigmoidal shape typical of type II BET [14,15] isotherms. Primary absorption isotherms from our study are given in Fig. 1 for three different temperatures. Although the BET construct is traditionally used to describe adsorption onto surfaces, it is useful for describing the absorption of water into the amorphous cellulosic matrix of paper fibers. Water bonds strongly at the three hydrogen

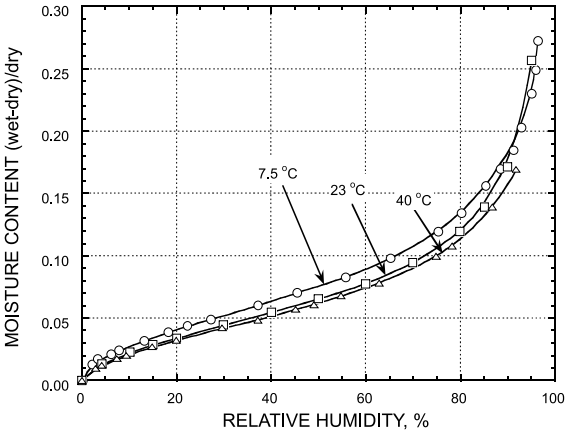

Fig. 1. The primary absorption isotherms for the laboratory materials at three different temperatures.

bonding sites on each of the glucose repeat units whether they lie on the gas–solid interface or are inside the amorphous matrix. Additional water solvates the matrix as "unbound" water to form a gel.

The mass fraction of water absorbed on a dry fiber basis is

$$\frac{\omega_{\mathrm{mc}}}{\omega_{\mathrm{mono}}} = \frac{Ca_{\mathrm{w}}}{(1-a_{\mathrm{w}})[1+(C-1)a_{\mathrm{w}}]} \tag{20}$$

where the activity of the water vapor is identical to the relative humidity. The weight fraction of water in the pores is related to the activity by

$$\omega_{\mathrm{p}} = \frac{M_{\mathrm{w}}p^{\mathrm{sat}}a_{\mathrm{w}}}{M_{\mathrm{a}}P} \tag{21}$$

In terms of the mass fraction on a total mass basis, the equilibrium moisture content is

$$\omega_{\mathrm{eq}} = \frac{\omega_{\mathrm{mc}}}{\omega_{\mathrm{mc}}+1} \tag{22}$$

The equilibrium constant C is expressed in terms of the enthalpy of adsorption of water onto the primary hydrogen binding sites and the heat of condensation

$$C \cong \exp\left[-\frac{(\Delta H_{\mathrm{prim}} - \Delta H_{\mathrm{cond}})}{RT}\right] \tag{23}$$

Eq. (20) agrees well with equilibrium moisture content data for relative humidities below 40%. Between 10% and 80%, better agreement is found with the semi-empirical GAB isotherm [16], in which the water activity in Eq. (20) is replaced by ka_{w}, where k is typically less than unity for cellulosic materials. At higher relative humidities, a term of the form $Aa_{\mathrm{w}}/(1-a_{\mathrm{w}})^2$ is added to Eq. (20) to fit the upper portions of the isotherm.

The mass transport equations are made non-dimensional by introducing new variables

$$\psi = \frac{D_{p,0}t}{\tau_p l^2}, \quad \zeta = \frac{z}{l}, \quad D_p^* = \frac{D_p}{D_{p,0}}, \quad K_{eq} = \frac{\omega_{f,\infty} - \omega_{f,0}}{\omega_{p,\infty} - \omega_{p,0}} \tag{24}$$

and

$$\omega_p^* = \frac{\omega_p - \omega_{p,0}}{\omega_{p,\infty} - \omega_{p,0}}, \quad \omega_f^* = \frac{\omega_f - \omega_{f,0}}{\omega_{f,\infty} - \omega_{f,0}},$$
$$\omega_{eq}^* = \frac{\omega_{eq}(\omega_p) - \omega_{f,0}}{\omega_{f,\infty} - \omega_{f,0}} \tag{25}$$

The new weight fractions, ω^*, vary between 0 and 1 during a moisture sorption transient. Assuming the condition in Eq. (4), Eqs. (1) and (2) become

$$\frac{\partial \omega_p^*}{\partial \psi} = \frac{\partial}{\partial \zeta}\left(D_p^* \frac{\partial \omega_p^*}{\partial \zeta}\right) - \beta_p K_{eq}(\omega_{eq}^* - \omega_f^*) \tag{26}$$

and

$$\frac{\partial \omega_f^*}{\partial \psi} = \beta_f(\omega_{eq}^* - \omega_f^*) \tag{27}$$

where

$$\beta_p = \frac{3a_s a \tau_p}{\varepsilon}\left(\frac{l}{a}\right)^2 \left[\frac{a\rho_f D_p^* D_f}{b\rho_p D_p + a\rho_f D_f(\partial\omega_{eq}/\partial\omega_p)|_{x=a}}\right] \quad \text{and}$$
$$\beta_f = \frac{\varepsilon\rho_p}{(1-\varepsilon)\rho_f}\beta_p \tag{28}$$

where the quantity $a_s a/\varepsilon$ is unity based on the assumption of a slab-like pore shape described above. The boundary conditions given by Eqs. (5) and (6) become

$$\left.\frac{\partial \omega_p^*}{\partial \zeta}\right|_{\zeta=0} = 0 \tag{29}$$

and

$$\left.\frac{\partial \omega_p^*}{\partial \zeta}\right|_{\zeta=1} = -N_{Bi,m}[\omega_p^*|_{\zeta=1} - \omega_\infty^*(\psi)] \tag{30}$$

where

$$N_{Bi,m} = \frac{\tau_p K_{m,s} l}{\varepsilon D_p} \tag{31}$$

which is the Biot number at the surface of the sheet. The initial conditions given in Eqs. (7) and (8) become

$$\omega_p^*(\zeta, 0) = \omega_f^*(\zeta, 0) = 0 \tag{32}$$

In the case of steady state moisture transport through a sheet, the fibers are everywhere in equilibrium with the surrounding pores. Hence, $\omega_f = \omega_{eq}(\omega_p)$. Assuming the humidity difference across the sheet is not large and the isotherms are linear over that range then the steady state moisture flux in the z-direction is

$$j_{ss} = -\left[\frac{\rho_p \varepsilon D_p}{\tau_p} + \frac{K_{eq}\rho_f(1-\varepsilon)D_f}{\tau_f}\right]\frac{\partial \omega_p}{\partial z}$$
$$= -\rho_p D_{eff}\frac{\partial \omega_p}{\partial z} \tag{33}$$

where the derivative is estimated from the humidity difference across the sheet divided by the thickness.

The thermal energy balance in the pores is

$$\rho_p \widehat{C}_{p,p}\frac{\partial T_p}{\partial t} = \frac{1}{\tau_p}\frac{\partial}{\partial z}\left(k_p \frac{\partial T_p}{\partial z}\right) - \frac{a_s K_{h,i}}{\varepsilon}(T_p - T_f) \tag{34}$$

and in the fibers is

$$\rho_f \widehat{C}_{p,f}\frac{\partial T_f}{\partial t} = \frac{1}{\tau_f}\frac{\partial}{\partial z}\left(k_f \frac{\partial T_f}{\partial z}\right) - \rho_f \Delta H_{abs}\frac{\partial \omega_f}{\partial t}$$
$$+ \frac{a_s K_{h,i}}{(1-\varepsilon)}(T_p - T_f) \tag{35}$$

The heat of absorption is a function of the moisture content of the sheet. Water condenses with different energies depending on whether it is absorbed at a primary hydrogen bonding site or as unbound water. Therefore, the heat of absorption is

$$\Delta H_{abs} = (\Delta H_{prim} - \Delta H_{cond})\frac{\omega_{prim}}{\omega_{mc}} + \Delta H_{cond} \tag{36}$$

The ratio of water bound to the primary sites compared to the total absorbed water can be determined from BET theory

$$\frac{\omega_{prim}}{\omega_{mc}} = 1 - a_w = 1 - \frac{1}{2(C-1)}\left[C\left(1 - \frac{\omega_{mono}}{\omega_{mc}}\right)\right.$$
$$\left. - 2 + \sqrt{C^2\left(1 - \frac{\omega_{mono}}{\omega_{mc}}\right)^2 + 4C\frac{\omega_{mono}}{\omega_{mc}}}\right] \tag{37}$$

where this is now expressed in terms of the moisture content. This result is identical for the GAB isotherm, other than that a_w is replaced by ka_w in Eq. (37).

In a procedure similar to the one above used to derive $K_{m,i}$, the overall interphase heat transfer coefficient is shown to be

$$K_{h,i} = \frac{3k_p k_f}{bk_p + ak_f} \tag{38}$$

Using the values of the material properties listed in Tables 1 and 2, it is shown that

$$\frac{a_s l^2 \tau_p K_{h,i}}{\varepsilon k_p} \gg 1 \tag{39}$$

from which it follows that $T_p \cong T_f$ at all z. Therefore, using the assumption that $T_p = T_f = T$, and defining the effective thermal conductivity as

$$k_{eff} = \frac{\varepsilon k_p}{\tau_p} + \frac{(1-\varepsilon)k_f}{\tau_f} \tag{40}$$

Eqs. (34) and (35) may be combined into a single equation

Table 1
Material and transport properties common to all experiments

Parameter	Value
T_∞	296 K
ρ_f	1550 kg/m^3
ρ_p	1.18 kg/m^3
ρ_s	633 kg/m^3
ε	0.6
b	1.3 μm
$a_s a/\varepsilon$	1
D_p	2.53×10^{-5} m^2/s
$\widehat{C}_{p,p}$	1.004×10^3 J/kg/K
k_p	0.026 J/m/s/K
k_f	0.615 J/m/s/K
$K_{m,s}$	2.27×10^{-3} m/s
ΔH_{cond}	-2.453×10^6 J/kg
ΔH_{prim}	-3.164×10^6 J/kg
ω_{mono} (for ω_{eq})	0.04513
C (for ω_{eq})	11.55
k (for ω_{eq})	0.79
$K_{h,s}$	2.45 J/m^2/s/K
$K_{h,i}$	3.37×10^4 J/m^2/s/K
$\widehat{C}_{p,f}$	1.72×10^3 J/kg/K

Table 2
Experimental conditions and additional material and transport properties used to characterize a single sheet absorption transient

Parameter	Value
T_∞	296 K
RH_i	10%
RH_f	60%
$\omega_{p,i}$	1.78×10^{-3}
$\omega_{p,f}$	0.01057
$\omega_{f,i}$	0.0244
$\omega_{f,f}$	0.0716
K_{eq}	5.36
t_{ramp}	21 min
l	0.3445 mm
a	2.26 μm
ε/τ_p	0.07
b/a	11.33
l/a	152.4
τ_p	2.0
D_f	3.8×10^{-14} m^2/s
β_p	2.43×10^{-2}
β_f	2.77×10^{-5}
$N_{Bi,m}$	0.442

$$[\varepsilon\rho_p\widehat{C}_{p,p} + (1-\varepsilon)\rho_f\widehat{C}_{p,f}]\frac{\partial T}{\partial t} = \frac{\partial}{\partial z}\left(k_{eff}\frac{\partial T}{\partial z}\right) - (1-\varepsilon)\rho_f\Delta H_{abs}\frac{\partial \omega_f}{\partial t} \quad (41)$$

Again, using the values for the material properties in Table 1, it is found that

$$(1-\varepsilon)\rho_f\widehat{C}_{p,f} \gg \varepsilon\rho_p\widehat{C}_{p,p} \quad (42)$$

Applying this and introducing the dimensionless temperature and thermal conductivity

$$\theta = \frac{T}{T_0} \quad \text{and} \quad k^*_{eff} = \frac{k_{eff}}{k_{eff,0}} \quad (43)$$

Eq. (41) becomes

$$\frac{\partial\theta}{\partial\psi} = \frac{\tau_p\rho_p\widehat{C}_{p,p}}{(1-\varepsilon)\rho_f\widehat{C}_{p,f}N_{Le}}\frac{\partial}{\partial\zeta}\left(k^*_{eff}\frac{\partial\theta}{\partial\zeta}\right) - \frac{\Delta H_{abs}}{\widehat{C}_{p,f}T_0}(\omega_{f,\infty}-\omega_{f,0})\beta_f(\omega^*_{eq}-\omega^*_f) \quad (44)$$

where Eq. (27) was applied in the last term and the Lewis number is defined as

$$N_{Le} = \frac{\rho_p\widehat{C}_{p,p}D_{p,0}}{k_{eff,0}} \quad (45)$$

At the surface of the sheet

$$-k_{eff}\left.\frac{\partial T}{\partial z}\right|_{z=l} = K_{h,s}[T|_{z=l} - T_\infty(t)] \quad (46)$$

which becomes

$$\left.\frac{\partial\theta}{\partial\zeta}\right|_{\zeta=1} = -N_{Bi,h}(\theta|_{\zeta=1} - \theta_\infty) \quad (47)$$

The Biot number for heat transfer is defined as

$$N_{Bi,h} = \frac{K_{h,s}l}{k_{eff}} \quad (48)$$

where $K_{h,s}$ is estimated from the measured value of $K_{m,s}$ using the empirical relation

$$K_{h,s} \cong K_{m,s}\left(\frac{k_p}{D_p}\right)^{2/3}(\rho_p\widehat{C}_{p,p})^{1/3} \quad (49)$$

valid for $10^3 < N_{Re,L} < 3 \times 10^5$ [17].

Eqs. (26), (27) and (44) are solved numerically using orthogonal collocation for the spatial derivatives with five collocation points at $\zeta = 0.1834$, 0.5255, 0.7967, 0.9603 and 1.0 (see Finlayson [18]). A semi-implicit Bulirsch–Stoer method with variable time-stepping described in Press et al. [19] was used for the time integration with a maximum Jacobian error of 10^{-10} and a maximum relative error of 10^{-8}.

3. Experimental procedures

Five different types of experiments were conducted in order to assess the fundamental mass and heat transfer properties of paper sheets. All experiments were conducted with laboratory sheets made of Kraft processed and bleached red alder (Alnus rubra) pulp.

The first experiment involved the measurement of equilibrium moisture content isotherms at three temperatures. These measurements were performed in an environmental chamber, a replicate of which is described by Chatterjee et al. [20]. The humidity inside the chamber was controlled to a precision of 0.2% and measured to an accuracy of 1.0% (2% above 90% RH). The temperature was maintained to within 0.5 °C of the set point by placing the entire chamber in a temperature controlled room. The moisture content of a sheet was measured by suspending it by a wire from a Mettler PM200 analytical balance placed outside of the chamber to an accuracy of 1.0 mg. Moisture contents were measured this way to an accuracy of 5×10^{-4} when expressed as the weight fraction of the dry fiber. In a typical absorption isotherm measurement, the sheet was first dried at 0% RH at the temperature of interest to obtain the equilibrium dry mass. The results of the primary absorption experiments are given in Fig. 1.

In a second set of experiments, the transient moisture content of a single sheet was measured in response to a change in humidity. The sheet was first preconditioned to start the transient on the appropriate isotherm. The humidity was then brought from the starting value to the new value along a linear ramp of duration t_{ramp} and held there for the remainder of the experiment.

In a third set of experiments, the z-direction moisture profiles were measured during a moisture absorption transient using a stacked composite constructed from six identical sheets. One side of the composite was covered with aluminum foil so that moisture could penetrate only the uncovered side. All sheets were held in close contact by slightly bending the composite. A moisture transient was initiated with the composite sheet in the same way as for a single sheet transient. However, at a certain time during the transient, the composite sheet was quickly removed from the environmental chamber, disassembled, and each sheet was placed in its own separate polyethylene bag. After all sheets were bagged, they were removed one at a time and weighed on a Mettler PM200 balance in a 50% RH room. To capture the weight of the sheet just as it was removed from the bag, the weight data was collected through the balance RS232 port at 1 Hz for two minutes. The moist weight of the sheet was determined by extrapolating the data back to the time the sheet was removed from the bag. Because the composite sample was destroyed to obtain data, the experiment was repeated several times with identical new sheets, in each case stopping at different times after the beginning of the transient.

In a fourth experiment, the effective diffusivity of moisture in paper was measured using a diffusion stack, a modified form of one proposed by Lescanne et al. [7]. It consisted of a container of water with the same diameter as the circular sheets above which several sheets were stacked, each separated by rings. The rings between the paper samples were 5 mm in height and 150 mm in inner diameter. Unshielded temperature and humidity probes (Omega, HX93C with accuracies of 2.5% RH and 0.6 °C) were placed in the void spaces between each sheet. To prevent moisture transport through the walls, the container and rings were constructed of high density polyethylene and the edges of the sheets were waxed. The steady state moisture flux through the sheets, j_{ss} was found by measuring the rate of mass loss of water from the stack while in the humidity chamber. After the moisture flux was measured, the humidity between each sheet was measured to obtain the z-direction moisture gradients.

In the final set of experiments, the surface temperature of a sheet was measured using a non-contact infrared pyrometer (Omega, OS65-V-R1-1) during sorption and desorption transients. A 50×50 mm sheet was suspended in a frame so that both sides of the sheet were unobstructed from air flow. The pyrometer was focused onto a 12 mm diameter spot at the center of the sheet. Since paper is a layered material, the temperature measured is that of the surface fibers. The surface temperature of the sheet was measured to a precision of 0.04 °C.

4. Moisture transport results

The value of $\tau_{\text{p}}/\varepsilon$, which appears in Eq. (28) and required for the analysis of transients, can be approximated by measuring the z-direction effective diffusivity using a steady-state diffusion stack. The effective diffusivity experiment was performed with the diffusion stack assembly enclosed in a 23 °C and 10% RH environment. After accounting for the moisture gradients across the air gaps between the sheets, a mean value of $D_{\text{eff}} = 1.8 \times 10^{-6}$ m^2/s (st. dev. $= 7 \times 10^{-7}$ m^2/s) was found for the six sheets in the stack. This magnitude suggests that most of the moisture transport through the sheet occurs by vapor diffusion through the pore spaces. Using Eq. (33), $\varepsilon/\tau_{\text{p}}$ is found to have a value of 0.07, assuming that all moisture diffuses through the pores and none through the fibers.

With the value for $\varepsilon/\tau_{\text{p}}$, Eqs. (3) and (19) are used to evaluate $\varepsilon = 0.14$, $\tau_{\text{p}} = 2.0$, and $b/a = 11.33$. The values for these parameters obtained from the effective diffusivity measurements differ significantly from those derived from physical measurements, as listed in Table 1. The small value of $\varepsilon/\tau_{\text{p}}$ suggests that the effective diffusional thickness of the fiber wall is much larger than its physical cross-section, due to the highly consolidated state of the fibers in the sheet, and that not all pores participate as paths for moisture diffusion, either due to dead-end pores or closed lumen spaces.

The diffusivity of water into the fibers is estimated by comparing the results of a transient sorption experiment

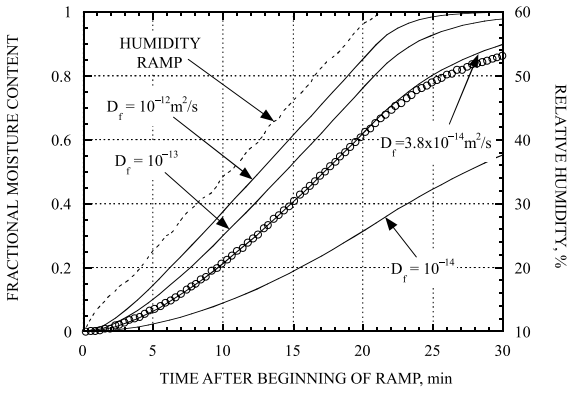

Fig. 2. Absorption transient compared with theoretical estimates at various values of the diffusivity of water in the fibers. The humidity is ramped from 10% to 60% RH in 21 min along a nearly linear portion of the isotherm.

with the mass transport model (assuming isothermal conditions) and choosing a value for D_f which match the experiment. In the experiment, the moisture content of a sheet, initially at equilibrium with 10% RH vapor, is measured as the relative humidity is changed in a 21 min linear ramp from 10% to 60% and then held constant at 60%. The comparison between the model and experiment is shown in Fig. 2 where the parameters used for the calculations are listed in Table 2. For the calculation of β_p, given by Eq. (28), the term inside the brackets represents fiber-to-pore mass transport and so a value of $b/a = 11.33$, determined from the effective diffusivity measurements, is used there. The terms outside the brackets represent the relative volumes of the pores and fibers and so are evaluated based on the porosity returned by the sheet density. For the pore tortuosity, a value of $\tau_p = 2.0$ is used. As Fig. 2 shows, the best fit of the data is given by a choice of $D_f = 3.8 \times 10^{-14}$ m^2/s. This value is consistent with a polymer gel model of the fiber wall, reflecting the effects of a low diffusivity through the amorphous polymer gel and the limited amount of amorphous polymeric material in the semicrystalline solid. Presumably, the small amorphous fraction results in a tortuous path for diffusion of absorbed water through the fiber wall, reducing the diffusivity.

The composite sheet experiments are used to verify the performance of the mass transport model. The material parameters used are listed in Table 3. The results of this experiment and accompanying simulation results are shown in Fig. 3. This figure shows the moisture content of each of the six sheets that make up the experimental composite at six different times after the start of a 33.5 min ramped transient from 10% to 70% RH. The moisture content data are plotted at the position of the mid-plane of each sheet.

Table 3
Experimental conditions and additional material and transport properties used to characterize the composite sheet experiment

Parameter	Value
T_∞	296 K
RH_i	10%
RH_f	70%
$\omega_{p,i}$	1.78×10^{-3}
$\omega_{p,f}$	0.01231
$\omega_{f,i}$	0.0380
$\omega_{f,f}$	0.0871
K_{eq}	4.66
t_{ramp}	33.5 min
l	2.024 mm
ε	0.23
$D_{w,f}$	2.3×10^{-14} m^2/s
β_p	0.819
β_f	1.87×10^{-4}
$N_{Bi,m}$	2.60

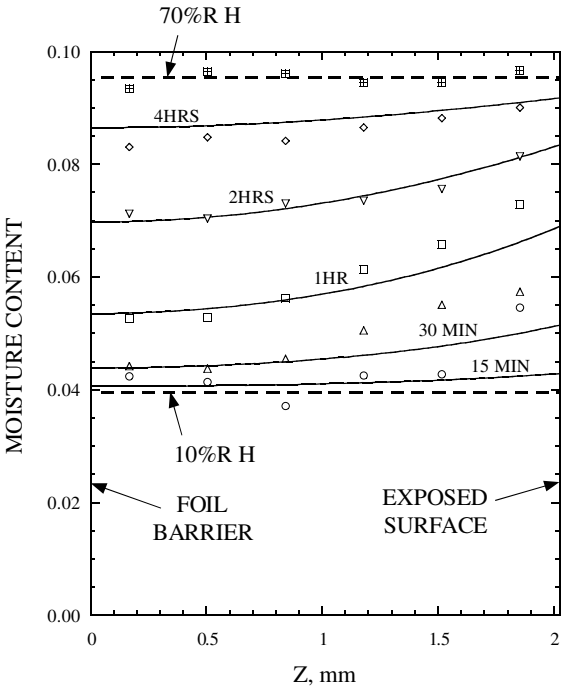

Fig. 3. Moisture content gradients in a composite at various times during an absorption transient. One side of the six sheet composite stack is covered with a water impermeable foil barrier and the other side is exposed to a changing humidity environment.

The composite sheet data confirm the model prediction that at no time are the moisture gradients large, even for this very thick composite sheet. These data also demonstrate that the moisture content of the surface does not immediately equilibrate with the surrounding

environment. These effects are caused by the large resistances to mass transfer in the laminar boundary layer outside the sheet and within the fiber walls and the rapid moisture transport through the pore spaces. Furthermore, the diffusivity of water through the fibers predicted in the analysis of the z-direction gradients in the composite sheet experiment is consistent with the diffusivity predicted by analysis of the transient uptake by single sheets.

5. Heat transport results

The heat of sorption, required by the transient heating analysis, is found as a function of moisture content by applying the Clausius–Clapeyron relation to the experimentally determined moisture content isotherms shown in Fig. 1. The heat of sorption at a given moisture content is found from the slope of $\ln(p_w)$ versus $1/T$ where p_w is the partial pressure of water. These are plotted at various moisture contents in Fig. 4.

Eqs. (36) and (37) are also plotted in Fig. 4 for two different sets of parameters. Although a value of $C = 10$ is typical of the experimental paper sheets used in this study, the fit using $C = 30$ is used in subsequent calculations because it fits the heat of absorption data more accurately at low moisture contents. Values for the material parameters found in Eqs. (36) and (37) are contained in Table 1.

The surface temperature measured during an absorption transient is shown in Fig. 5. The heating occurs in two stages, one near the beginning and one near the end for the linear ramp in the surrounding humidity. The combined heat and mass transport model demonstrates

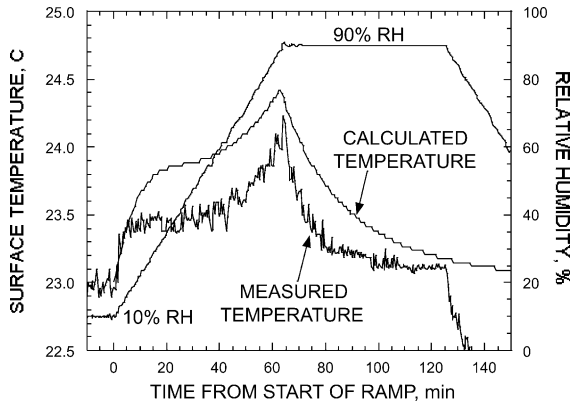

Fig. 5. Theoretical fit of surface temperature in response to a 1 h ramp from 10% to 90% RH.

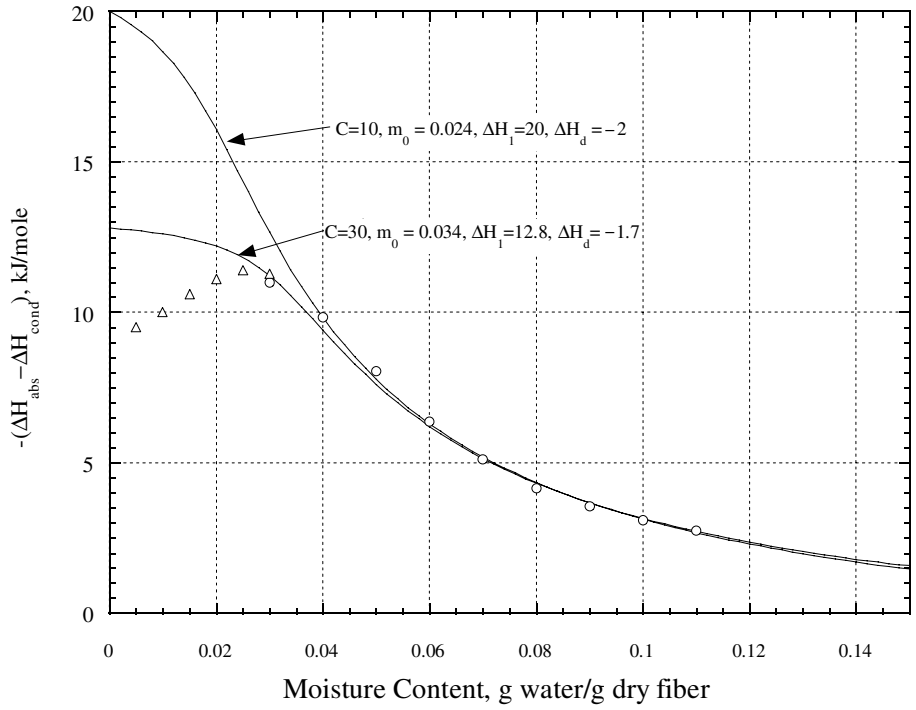

Fig. 4. Differential heat of absorption minus differential heat of condensation as a function of the moisture content. The triangles and circles are evaluated from primary absorption isotherm data and the solid lines represent theoretical fits for two different sets of parameters.

Table 4
Experimental conditions and additional material and transport properties used to characterize the surface temperature of a sheet during moisture sorption

Parameter	Value
T_∞	296 K
RH_i	10%
RH_f	90%
$\omega_{p,i}$	1.78×10^{-3}
$\omega_{p,f}$	0.0158
$\omega_{f,i}$	0.0244
$\omega_{f,f}$	0.161
K_{eq}	4.66
t_{ramp}	63 min
l	0.3445 mm
A (for ω_{eq})	2.5×10^{-3}
ω_{mono} (for ΔH_{abs})	0.034
C (for ΔH_{abs})	30
k_{eff}	0.181
$N_{Bi,m}$	0.13
$N_{Bi,h}$	0.1
N_{Le}	0.0612

that this two-stage behavior results from the non-linearity in both the moisture content isotherm and the heat of absorption. The surface temperature predicted by the solution of Eqs. (44) and (47), using the material properties listed in Tables 1 and 4, is also shown in Fig. 5. Since the energy balance is coupled with the moisture balances, the heat transport equations are solved simultaneously with the mass transport problem described by Eqs. (26), (27) and (30). The non-linear moisture content isotherm, described by the GAB modified form of Eq. (20), and the non-linear heat of absorption, described by Eqs. (36) and (37), again in the GAB form, are used in this analysis. The calculated results accurately predict the shape of the two stage heating behavior. They also predict the drop in temperature immediately following the completion of the humidity ramp. The mismatch in magnitude of the predicted temperature response may be due to inaccuracies of the Biot number for heat transfer given in Eq. (48) or use of a heat of absorption that is slightly higher than measured at low moisture contents.

6. Discussion

There exists a considerable body of literature regarding the nature of moisture sorption in wood pulp fibers. Some of this work presupposes that water adsorbs onto the surfaces of micropores between the fibrils of cellulosic fibers. This work, in contrast, relies on an absorption model, which assumes that most water held by cellulose based fibers resides in the amorphous regions of the various hygroscopic components as a mixture in a swollen polymer matrix.

The absorption model is well supported by experimental evidence. The water associated with the primary hydrogen bonds of the hygroscopic components in the cell wall represents far more water than can be adsorbed onto the available surfaces. Analysis of the absorption isotherm at 23 °C shown in Fig. 1 returns a value of 0.0374 kg of water associated with the primary bonds per kg of dry fiber. Using an adsorbed surface area of 0.125 nm^2 for water molecules, this gives an adsorption area of approximately 1.56×10^5 m^2/kg. Electron micrographs of swollen pulp fibers show no more than 1.5×10^4 m^2/kg of exposed surfaces [21] but this is more likely on the order of 3×10^3 m^2/kg [22]. Furthermore, nitrogen adsorption typically gives values of 5×10^2–1×10^3 m^2/kg for the surface area of dry, unswollen pulp fibers. The glucose repeat unit of cellulose has a length and width of 1.3 nm and so if all three available hydroxyl groups are exposed on one surface, they would represent only about 20% of the exposed physical area for forming primary hydrogen bonds. Therefore, even in the most extreme case of 1.5×10^4 m^2/kg for the exposed surface area, only about 2% of primary sorption of water occurs as adsorption onto surfaces. The vast majority of primary sorbed water must solvate the amorphous regions, diffuse through the entangled cellulose polymer and bind directly to hydroxyl groups inside the solid matrix.

Additional evidence for the absorption model comes from the mechanical changes of fibers upon exposure to humidity. When penetrating the amorphous regions, water acts as both a plasticizer and swelling agent. This leads to dramatic reductions in fiber stiffness and changes in fiber dimensions. The first absorbed water breaks existing intra and interchain hydrogen bonds that make the dry cellulose amorphous matrix rigid, and replaces them with more flexible water bridges, initially only one water molecule in length. Additional adsorbed water either adds to these bridges or solvates the matrix as free water, forming a gel. At a humidity of 80%, the amount of absorbed water represents three times the water associated with primary absorption, or nine water molecules per glucose repeat unit of the cellulose. Since the repeat unit has a molecular mass of 162 kg/kmol, the amorphous regions are swollen to a moisture content of 50% by weight, causing a considerable swelling and weakening of the amorphous regions. Furthermore, at high moisture contents, more free water is available for diffusion and presumably the diffusivity is higher [23].

The isotherms provide insight into the nature of the cellulose–water gel state. At low moisture contents, absorption equilibrium is dominated by the enthalpic interactions associated with the disruption of cellulose-to-cellulose hydrogen bonds and reformation of water-to-cellulose hydrogen bonds. Since these interactions are strong, moisture is preferentially drawn to these sites

and the moisture content is considerably higher than the water activity. This positive deviation from ideality gives rise to the characteristic type II isotherm shape where the isotherms lay above ideal solution curve. As the moisture content increases and more primary sites are occupied, a larger fraction of water absorbs as free water solvating the polymer and creating a gel. Here, the water–cellulose interaction is now dominated by entropic restrictions to the motion of the polymer chains in the solution. These restrictions act to exclude moisture and the moisture content drops below the water activity. Hence, the isotherms are overpredicted by the extension of the BET analysis to this region. As the activity increases to unity (100% RH), the amorphous cellulose is not completely solvated because the cellulose in the amorphous regions is physically held together by intrachain links to the non-solvating crystalline regions. Hence, the fibers swell to their saturation point and exclude any additional water. In the thermodynamic sense, this can be viewed as phase splitting between the solvated polymer phase and the pure solvent phase, a possibility for polymer solutions with a Flory–Huggins interaction parameter greater than 0.5.

Based upon the simulation and experimental results presented here, the value of the single fiber diffusivity, D_f, is suggested to be 3×10^{-14} m^2/s. This is a very small value but one that is consistent with a polymer gel model of the fiber wall. The value of the diffusivity reflects the combination of a small diffusivity through the amorphous polymer gel and the limited amount of amorphous cellulosic polymer in the semi-crystalline solid of the fiber wall.

Although the simple combined mass and thermal transport model presented here does well, improvements are needed in the way in which the porous system is represented. Measurements of sheet porosity based on the density differ from the value of porosity which is required to represent the diffusive system. This suggests that a significant portion of the pore system is not a pathway for moisture transport. This portion of the air space may either be inaccessible volume inside partially collapsed fibers or dead-end pores. In addition, for typical sheet porosities on the order of 0.5, there are several interfiber bonds along the length of each fiber. This means that the proportion of external surface area of a fiber directly exposed to the diffusive pore system is much smaller than the geometry of a single fiber would suggest. One would expect then that the diffusive distances into the fiber wall would be greater than the wall thickness. All of this suggests that one-dimensional geometries assumed in the model are not entirely adequate. One can envision a model where there is a passive pore space, an active pore space, fiber surface area which is exposed to the active pore space and surface area exposed to the passive pore space.

7. Conclusion

The goals of this work were to clarify the mechanisms by which paper sheets absorb moisture from humid air and to measure the fundamental variables of this mass and heat transport process. When the humidity around a paper sheet increases, the sheet absorbs moisture and its temperature increases. The rate of that moisture sorption is dependent on the magnitude of three mass transport resistances. These are the laminar boundary layer above the surface of the sheet, the quiescent air filled pores between the fibers of the sheet, and the pore-to-fibers region. In this work, moisture transport in paper was modeled to account for these three resistances and they were related to fundamental mass transport and geometric parameters. The temperature behavior of the sheet during the sorption process is also explained by linking a heat transfer model to the mass transfer model. The measured surface temperature transients exhibit a two-stage rise in temperature during moisture absorption which is predicted by the coupled heat and mass transport model.

Acknowledgements

The authors express their sincere gratitude to Weyerhaeuser Company for support of this work. The experimental assistance of J.R. Riedemann is also gratefully acknowledged.

References

[1] N.L. Salmen, E.L. Back, Effects of temperature and moisture on the tensile properties of packaging papers, Papper ja Puu 8 (1985) 477–481.
[2] T. Uesaka, General formula for hygroexpansion of paper, J. Mat. Sci. 29 (1994) 2373–2377.
[3] K.J. Niskanen, S.J. Kuskowski, C.A. Bronkhorst, Dynamic hygroexpansion of paperboards, Nordic Pulp Paper Res. J. 12 (1997) 103–110.
[4] Z.V. Padanyi, Mechano-sorptive effects and accelerated creep in paper, in: Proc. Int. Paper Phys. Conf., vol. 2, TAPPI Press, Atlanta, 1991, pp. 397–411.
[5] C.C. Habeger, D.W. Coffin, The role of stress concentrations in accelerated creep and sorption-induced physical aging, J. Pulp Paper Sci. 26 (2000) 145–157.
[6] W.R. Foss, C.A. Bronkhorst, K.A. Bennett, J.R. Riedemann, Transient moisture transport in paper in the hygroscopic range and its role in the mechano-sorptive effect, in: Proc. Third Int. Symp. Moist. Creep Effects on Paper, Board and Containers, PAPRO, Rotorua, NZ, 1997, pp. 221–236.
[7] Y. Lescanne, C. Moyne, P. Perre, Diffusion mechanisms in a sheet of paper, in: A.S. Mujumdar (Ed.), Drying'92, Elsevier Science Publishers, Amsterdam, 1992.

[8] L. Nilsson, B. Wilhelmsson, S. Stenstrom, The diffusion of water vapour through pulp and paper, Drying Technol. 11 (1993) 1205–1225.
[9] J.-G. Salin, Mass transfer from wooden surfaces and internal moisture non-equilibrium, in: V. Rudolph, R.B. Keey (Eds.), Drying'94, vol. B, Gold Coast, Australia, 1994.
[10] M.J. Cunningham, A model to explain "anomalous" moisture sorption in wood under step function driving forces, Wood Fiber Sci. 27 (1995) 265–277.
[11] J. Fan, X. Wen, Modeling heat and moisture transfer through fibrous insulation with phase change and mobile condensates, Int. J. Heat Mass Transfer 45 (2002) 4045–4055.
[12] J. Fan, Z. Luo, Y. Li, Heat and moisture transfer with sorption and condensation in porous clothing assemblies and numerical simulation, Int. J. Heat Mass Transfer 43 (2000) 2989–3000.
[13] K.A. Akanni, J.W. Evans, I.S. Abramson, Effective transport coefficients in heterogeneous media, Chem. Eng. Sci. 42 (1987) 1945–1954.
[14] S. Brunauer, P.H. Emmett, E. Teller, Absorption of gases in multimolecular layers, J. Am. Chem. Soc. 60 (1938) 309–319.
[15] A.J. Stamm, Adsorption in swelling versus nonswelling systems, I. Contact area, Tappi 40 (1957) 761–765.
[16] R.B. Anderson, Modifications of the Brunauer. Emmett and Teller equation, J. Am. Chem. Soc. 68 (1946) 681–691.
[17] F. Kreith, M.S. Bohn, Principles of Heat Transfer, fourth ed., Harper and Row, New York, 1986, pp. 184–236.
[18] B.A. Finlayson, Nonlinear Analysis in Chemical Engineering, McGraw-Hill, New York, 1980, pp. 191–193.
[19] W.H. Press, S.A. Teukolsky, W.T. Vetterling, B.P. Flannery, Numerical Recipes, second ed., Cambridge University Press, Cambridge, 1992.
[20] S.G. Chatterjee, B.V. Ramarao, C. Tien, Water–vapour sorption equilibria of a bleached-kraft paperboard—a study of the hysteresis region, J. Pulp Paper Sci. 23 (1997) J366–J373.
[21] A.M. Scallan, The structure of the cell wall—a consequence of anisotropic inter-microfibrillar bonding, Wood Sci. 6 (1974) 266–271.
[22] D.H. Page, J.H. De Grace, The delamination of fiber walls by beating and refining, Tappi 50 (1967) 489–495.
[23] H. Radhakrishnan, S.G. Chatterjee, B.V. Ramarao, Steady-state moisture transport in a bleached kraft paperboard stack, J. Pulp Paper Sci. 26 (2000) 140–144.